Arabian Journal of Geosciences (2019) 12: 61
https://doi.org/10.1007/s12517-018-4189-8

ORIGINAL PAPER

Petrography and geochemistry of the Neoproterozoic sedimentary rocks from the Batal Formation of Spiti Basin: implication on provenance

Shivani Pandey[1] · Suraj K. Parcha[1] · Pankaj K. Srivastava[2]

Received: 11 October 2017 / Accepted: 21 December 2018 / Published online: 15 January 2019

Abstract

The petrography and geochemistry of the siliciclastic rocks of Batal Formation, Spiti Basin were studied to define the provenance, tectonic setting, and depositional environment. Petrographical studies show that the percentage of quartz in sandstone varies from 70 to 80%, whereas in siltstone and shale, it varies from 50 to 60%. Similar pattern of chondrite-normalized REE, with enriched LREE, depleted HREE, and a negative Eu anomaly, suggests that the source rock is of felsic type. Significant correlation between Zr versus Yb and ΣHREE indicates that these sediments are influenced by sediment recycling. The Ni/Co and Cu/Zn ratios suggest that sediments were deposited under low to moderate oxygenated conditions, while the CIA values and A-CN-K plot reflect moderate to intense weathered source area with the presence of clay minerals derived during the cold period. The major element–based multidimensional tectonic discrimination diagrams suggest an active marginal setting for the sediments of Batal Formation. Further, the discrimination diagrams equally suggest that these sediments were derived from sedimentary provenance and to some extent from the felsic igneous provenance.

Keywords Neoproterozoic · Tectonic setting · Provenance · Depositional environment

Introduction

In the Spiti Basin, Batal Formation (Neoproterozoic) lies over the crystallines of Vaikrita Group in the Spiti Basin, and is primarily characterized by the rocks such as shale, siltstone, and sandstone. The clastic rocks of the Batal Formation are well exposed along the Batal-Chandratal road in this basin (Fig. 1). The geochemistry of clastic sediments has been used widely by various authors to infer the provenance, type of source rocks, and intensity of weathering (McLennan and Taylor 1991; Cullers 1994; Nagarajan et al. 2007a, b; Madhavaraju and Lee 2010; Armstrong-Altrin et al. 2013, 2015a, b, 2017, 2018; Madhavaraju 2015; Madhavaraju et al. 2016; Pandey and Parcha 2017). Siliciclastic sediment composition is mainly controlled by the source rock composition due to this major and trace element geochemistry of sediments that provide information about its origin as well as the weathering conditions in the source area (Ahmad et al. 2014; Armstrong-Altrin et al. 2015a). The main objectives of the present study are (1) to infer the provenance and tectonic setting and (2) to infer the paleoweathering and depositional condition. To achieve the objectives, major, trace, and rare earth element geochemistry of the Batal Formation was carried out.

Study area

Spiti Basin lies in the Lahaul-Spiti district of Himachal Pradesh, northern India. The Spiti Basin forms a part of the Spiti-Zanskar Basin that belongs to the geotectonic zone of the Tethyan Himalaya, and together, they make the largest basin in the Indian Tethys Himalaya. The basin is bounded by Indus-Tsangpo Suture Zone (ITSZ) in the north and metamorphic basement of the Central Crystalline zone in the south. The Paleozoic sequence in Spiti Basin is well exposed in the Parahio, Pin, Kunzum La-Takche, and Chandratal sections. The present studied section is exposed along the track route at 32° N and 77° E in between Batal and Chandratal (Fig. 1).

✉ Shivani Pandey
pandeshivani@gmail.com

[1] Wadia Institute of Himalayan Geology, G.M.S Road, Dehra Dun 248 001, India

[2] University of Jammu, Jammu, India

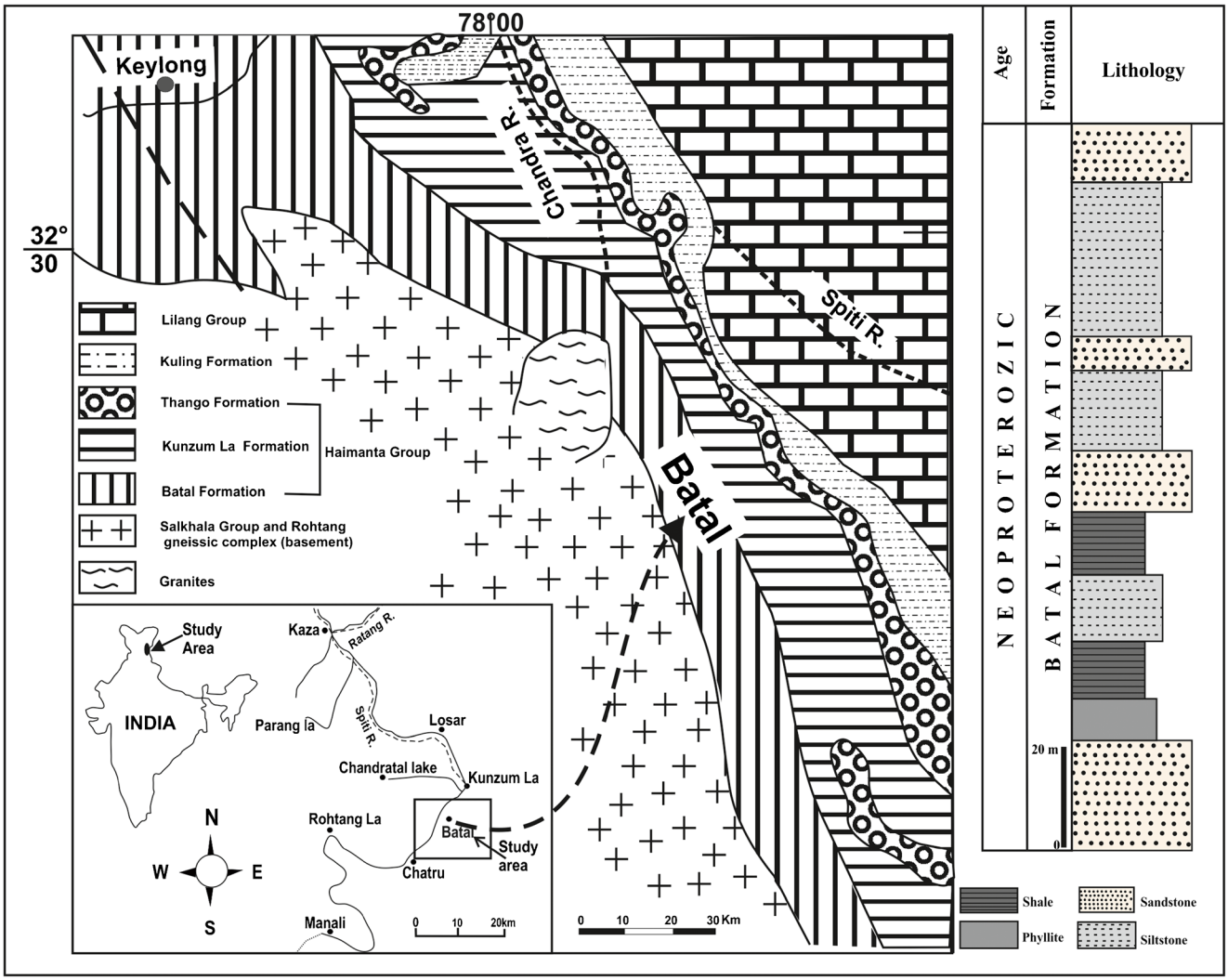

Fig. 1 Geological map and lithostratigraphic column of the Batal section exposed in the Batal-Chandratal section of the Spiti Basin

Stratigraphy and geological setting

Haimanta Group rests over the crystalline rocks of Vaikrita Group (Fig. 1). The term "Haimanta System" has been given by Griesbach (1891) to the sedimentary rocks above the metamorphic rocks of the Higher Himalaya (Vaikrita System). Hayden (1904) modified this term and suggested that whole of Haimanta System lies below an angular unconformity, which is no younger than late Ordovician. Srikantia (1981) adopted the term Haimanta Group instead of Haimanta System. Subsequently, Kumar et al. (1984) and Srikantia and Bhargava (1998) divided this group into Batal and Kunzum La formations. The contact between the Haimanta Group with underlying crystalline rocks of Vaikrita Group is still debatable. Thakur (1980) stated that the contact between these two units is gradational; on the contrary, Srikantia (1981) considers it to be as conformable. Dragnits (2000) and Myrow et al. (2006) considered it as gradational, whereas Bhargava (2008b) considered it as faulted. A gradual change in the lithology from the Vaikrita Group to Haimanta Group was observed during present studies; hence, we consider it to be of a gradational contact.

From the top of the Batal Formation except a record of cryptarch by Kumar et al. (1984) from the top of the Batal Formation, there is no record of fossils in this section so far. The age of Batal Formation remains a point of discussion among the workers due to lack of age diagnostic fossils. Srikantia (1981) and Srikantia and Bhargava (1998) assigned a terminal Proterozoic age to this formation on the basis of its stratigraphic position, while some workers consider it to be of a late Proterozoic age (e.g., Frank et al. 1995; Dragnits 2000; DiPietro and Pogue 2004). Bhargava (2008a) assigned Ediacaran-Early Cambrian age on the basis of overlying stratigraphy. Myrow et al. (2010) assigned Early Cambrian age based on the detrital zircon U-Pb age spectra of one sample from

the Spiti Basin. The Batal Formation can be assigned Late Neoproterozoic age based on its stratigraphic position.

Material and method

From the Batal Formation, 14 representative samples of sandstone, shale, siltstone, and phyllite were collected for the petrography and geochemical studies. Seven samples of sandstone, four samples of siltstone, two samples of shale, and one sample for phyllite were taken for the analyis. Petrographical and geochemical analyses of the samples were carried out at Wadia Institute of Himalayan Geology, Dehradun. Thin sections were studied under transmitted and reflected light using a Nikon Eclipse E600 POL microscope; they were prepared by cutting the rocks into small pieces using BUEHLER Delta Petrocut GEOLOGICAL CUTTER. One side of the rock wafers was grinded to make it smooth. The smooth side of the rock chips was mounted on glass slide using araldite/canada balsam. Wavelength dispersive XRF system (Siemens SRS 3000) was used to analyze major and trace elements. Ten grams of each sample was powdered in an agate mortar which was further analyzed using pressed powder pellet. For accuracy, analytical values were compared with the GSR-1 values by Govindaraju (1994). Major oxide and trace element data for each sample were recalculated to 100% after deduction of loss on ignition. The accuracy and precision for major oxides and trace elements was ± 2–5%. The REE data was analyzed by using inductively coupled plasma mass spectrometer (ICP-MS; PerkinElmer). Analysis was done by acid digestion which involves frequent treatment with HF-$HClO_4$ in 1:2 for 24 h in open system. REE data was normalized to chondrite values of Taylor and McLennan (1985). Eu/Eu* ratios were calculated based on formula given by Bau and Dulski (1996).

Result

Petrography

Sandstones are mostly fine- to medium-grained, poorly sorted, and contain angular to sub-angular grains of low to moderate sphericity. In sandstone, 80% of the total framework grains comprise of quartz (Fig. 2a), feldspar is generally less abundant than quartz and is ~ 10–15%, and remaining is lithic fragment. Monocrystalline quartz is present, and the edges of quartz grains are broken (Fig. 2a). Lithic fragments and heavy minerals like zircon are present (Fig. 2b). Matrix is commonly between 10 and 15%, which comprises of clay minerals, lithic and feldspathic fragments, fine-grained quartz, and mica. In siltstone, quartz is the most abundant mineral with almost 50–60%; the other minerals like feldspar, mica, and lithic fragments occur in less abundance. The unidirectional alignment of mica flakes indicates that the rocks were subjected to low-grade metamorphism (Fig. 2c–e). The siltstone consists ~ 20–30% of matrix, comprising of clay minerals, lithic and feldspathic fragments, fine-grained quartz, and micas. Fine-grained shale contain more than 50% of matrix supported by lithic fragments, mica, and poorly sorted quartz grains (Fig. 2f). Single sample of phyllite consists of feldspar, clay, and quartz with few ferruginous matter. At places, preferred orientation of micaceous minerals was also observed.

Major oxide

Major oxide data of clastic sediments collected from Batal Formation is listed in Table 1. In the studied samples, a large variation in chemical composition was observed. Sandstone contains moderate to high concentration of SiO_2 (64 to 84; average 74%), whereas siltstone and shale reflects low concentration of SiO_2 range from 54 to 62% with an average of 59 (Table 1); this composition indicates enrichment relative to the upper continental crust (UCC, 65.89 wt%) (Taylor and McLennan 1985). The Al_2O_3 content in sandstone shows a large range from 7 to 14%, whereas in the shale and siltstone, it ranges from 13 to 22% (Table 1). Elements such as Al_2O_3, Fe_2O_3, K_2O, and TiO_2 show a negative correlation with SiO_2 ($r = 0.91$ for Al_2O_3, 0.85 for Fe_2O_3, 0.79 for K_2O, 0.89 for TiO_2, respectively), which suggests that the rocks of studied section mostly contain clay sediments (Fig. 3). Concentration of high Al_2O_3 in sediments suggests their association either with clay or phyllosilicates in relationship with other elements (Nagarajan et al. 2017). Whereas, TiO_2 ($r = 0.88$) and K_2O ($r = 0.86$) exhibit positive correlation with Al_2O_3 (Fig. 4) which indicates that their association with clay mineral indicates chemical weathering in the source area (Nagarajan et al. 2017). It also suggests that TiO_2 is likely associated with phyllosilicates especially with illite and the enrichment of K_2O may be related to granitic/gneisses source (Dabard 1990; Armstrong-Altrin 2009, 2015). In the clastic sediments, if the value of SiO_2/Al_2O_3 ratio is > 5, it indicates sediment maturity (Armstrong-Altrin et al. 2012, 2013; Hernández-Hinojosa et al. 2018). The SiO_2/Al_2O_3 ratios vary from 1.7 to 10.9 in the rocks of Batal Formation, hence indicating a moderate textural maturity. In the Al_2O_3-Fe_2O_3-K_2O ternary plot, samples fall towards Al_2O_3 (Fig. 5) which indicate abundance of clay minerals in rocks (Wronkiewicz and Condie 1987).

Trace element

Trace element data of silisiclastic sediments collected from Batal Formation is listed in Table 2. Trace elements such as Co, Sc, Gb, and Y show a negative correlation with SiO_2 (for Co, $r = -0.86$; Sc, $r = -0.85$; Ga, $r = -0.94$; for Y, $r = -0.53$)

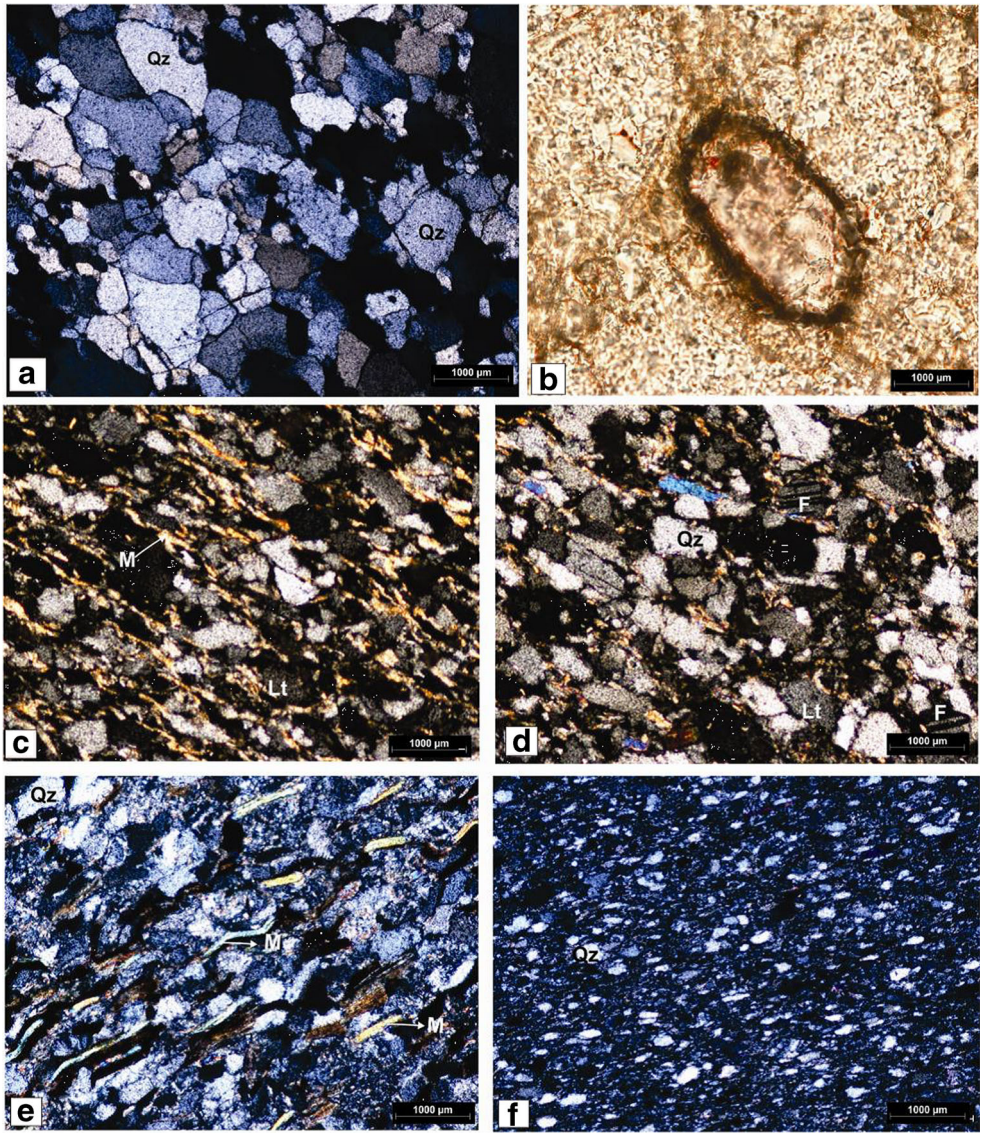

Fig. 2 **a**, **b** Photomicrographs of sandstone with presence of Zircon. **c**–**e** Siltstone with quartz, feldspar, and mica. Mica grains show alignment in one direction. **f** Photomicrographs showing shale with quartz and lithic fragments. Qz quartz, M mica, F feldspar, Lt lith

(Fig. 3). Positive correlation between Co, Rb, Sc, Nb with Al_2O_3 (for Co, $r = 0.69$; Rb, $r = 0.74$; Sc, $r = 0.91$; Nb, $r = 0.79$) (Fig. 4). Trace element such as Rb, Ga, Sc, and Nb shows positive correlation with K_2O (e.g., $r = 0.99$ for Rb; 0.88 for Ga; 0.81 for Sc; 0.79 for Nb, sample $n = 14$) suggesting that elements are primarily controlled by clay minerals (Fig. 6). The concentration of Zr/Rb ratio of the rocks shows wide variation from ~ 0.4 to 10.4 which reflects the grain size variations of the sediment, with higher values in the relatively coarse-grained units and lower values in fine-grained units.

REE

Rare earth element data of the samples collected from Batal Formation is listed in Table 3. The REEs are plotted against the chondrite-normalized REE pattern given by Taylor and McLennan (1985). The source rock signature in sedimentary rock is revealed by the pattern of REE, LREE/HREE ratio, and Eu anomaly (Cullers and Graf 1983; Fu et al. 2010; Madhavaraju et al. 2010; Armstrong-Altrin et al. 2013). It was observed that in the present study, all the samples show similar REE patterns with enriched LREE, depleted HREE, and a negative Eu anomaly (Fig. 7). The depletion of HREE, relative with LREE, was due to the lower concentration of heavy minerals (Nyakairu and Koeerl 2001). The siliciclastic rocks usually contain higher LREE/HREE ratios and negative Eu anomaly, whereas the basic rocks contain low LREE/HREE ratios and no Eu anomaly (Cullers and Graf 1983). The pattern of chondrite-normalized REE (including a negative Eu anomaly) and high LREE/HREE ratio (2.32–5.56) in the studied samples reveals that the source rock is of felsic type (Cullers et al. 1997). A statistically significant positive correlation was observed between ΣREE and Al_2O_3 and K_2O for the Batal Formation ($r = 0.93$ and $r = 0.52$, $n = 14$)

Table 1 Major oxide concentration data of the Neoproterozoic metasedimentary rocks of Batal Formation, Spiti Basin, Tethys Himalaya

Lithology	Sample	SiO_2	Al_2O_3	TiO_2	Fe_2O_3	MgO	Na_2O	K_2O	P_2O_5	MnO	CaO	LOI	K_2O/Na_2O	SiO_2/Al_2O_3	K_2O/Al_2O_3	CIA
Sandstone	B1	66.66	13.75	0.7	6.35	2.37	2.49	2.87	0.13	0.06	0.29	2.69	1.15	4.85	0.21	63.66
Sandstone	B2	78.7	9.49	0.47	3.53	1.43	3.02	1.84	0.1	0.05	0.78	1.62	0.61	8.29	0.19	54.63
Sandstone	B3	79.13	7.25	0.28	3.64	1.54	2.65	1.22	0.08	0.08	0.41	3.23	0.46	10.91	0.17	52.65
Phyllite	B4	45.87	25.64	1.07	10.79	3.36	0.79	5.43	0.13	0.08	0.1	5	6.87	1.79	0.21	64.75
Shale	B5	55.84	19.97	0.83	7.82	3.81	1.66	3.7	0.11	0.09	0.55	3.77	2.23	2.80	0.19	92.58
Siltstone	B6	61.37	18.24	0.74	6.04	2.05	2.54	3.77	0.1	0.05	0.14	3.39	1.48	3.36	0.21	81.75
Shale	B7	54.65	21.6	0.99	6.63	2.97	0.54	5.65	0.08	0.07	0.46	4.44	10.46	2.53	0.26	56.91
Sandstone	B8	69.9	11.85	0.5	6.53	2.5	2.21	2.03	0.12	0.07	0.47	2.62	0.92	5.90	0.17	73.99
Siltstone	B9	61.98	15.84	0.7	4.41	7.12	0.17	3.52	0.11	0.04	0.12	4.02	20.71	3.91	0.22	76.24
Sandstone	B10	84.42	12.23	0.26	2.46	6.7	0.12	0.74	0.08	0.03	0.08	2.17	6.17	6.90	0.06	78.53
Sandstone	B11	64.26	13.44	0.62	5.02	7.81	0.16	2.68	0.13	0.05	0.16	3.97	16.75	4.78	0.20	67.33
Siltstone	B12	61.92	12.61	0.46	9.24	6.9	2.6	0.25	0.11	0.07	0.15	3.19	0.10	4.91	0.02	80.41
Siltstone	B13	57.84	18.13	0.76	8.9	4.25	2.12	2.67	0.12	0.07	0.17	3.28	1.26	3.19	0.15	69.82
Sandstone	B14	73.31	10.25	0.7	4.62	3.08	3.28	1.2	0.17	0.05	0.28	1.9	0.37	7.15	0.12	72.40

suggesting that REE is mainly housed in detrital or heavy minerals (Armstrong-Altrin et al. 2017). Correlation between Zr versus Yb and ΣHREE was observed statistically significant as this reflects that the sediments are influenced by sediment recycling (Armstrong-Altrin et al. 2017).

Discussion

Major, trace, and REE concentrations in sediments have been used widely to know the provenance and environment conditions during deposition and tectonic setting of the source area and were defined by various discriminant diagrams (Bhatia 1983; Bhatia and Cook 1986; Roser and Korsch 1986; Sari and Koca 2012; Hernández-Hinojosa et al. 2018; Anaya-Gregorio et al. 2018). The geochemical composition of siliciclastic rocks is useful to define the provenance, weathering, and depositional condition, because these rocks are mainly controlled by the plate tectonic settings of their provenances, so the rocks from different tectonic settings have specific geochemical signatures (Bhatia 1983; Bhatia and Cook 1986; Roser and Korsch 1986; McLennan et al. 1993). In the present work, the geochemical studies of the Batal Formation rocks were undertaken aiming to provide a comprehensive and detailed analysis of provenance and depositional environment.

Verma and Armstrong-Altrin (2013) defined tectonic setting by using major element–based discrimination diagrams. They proposed discriminant function diagram based on major element to define the tectonic discrimination of siliciclastic sediments for high-silica [(SiO_2) adj = 63–95%] and low-silica [(SiO_2) adj = 35–63%] types, from three main tectonic settings: island or continental arc, continental rift, and collision. The continental arc and collision field represent active margin, whereas continental rift represents passive margin. Armstrong-Altrin and Verma (2005) evaluated this discrimination diagram and showed a low percentage success rate (0%–23%) for the Bhatia (1983) diagram and 31.5%–52.3% for the Roser and Korsch (1986) diagram. Further, this multidimensional diagram can be considered as a tool for successfully discriminating the tectonic setting of older sedimentary basins (Armstrong-Altrin 2015a). Recently, Hernández-Hinojosa et al. (2018), Armstrong-Altrin et al. (2017), Tobia and Aswad (2015), and Zaid (2015b, c) used the multidimensional discrimination diagram to study the tectonic setting of source region of clastic sediments based on geochemistry. In the present study, authors used major element–based discrimination diagrams proposed by Verma and Armstrong-Altrin (2013). It is observed that the rocks which contain high silica percentage plotted in the collision field (Fig. 8a) whereas at the same time, the rocks containing low silica percentage are also plotted in the collision field (Fig. 8b). On the basis of these high silica and low silica multidimensional diagrams (Fig. 8a, b), the present studied samples are plotted mostly in the collision field suggesting that the deposition of sediments took place in active continental margin environment.

To describe the provenance of sediments, Roser and Korsch (1986) define four different major group of rocks; they are mafic igneous provenance (P1), intermediate igneous provenance (P2), felsic igneous provenance (P3), and quartzose sedimentary provenances (P4). In the studied discriminate diagram, samples mostly represent the quartzose sedimentary provenance and to some extent the felsic igneous provenance, suggesting that sediments may derived mainly from the silica-rich sedimentary provenance (Fig. 9) with subordinate felsic

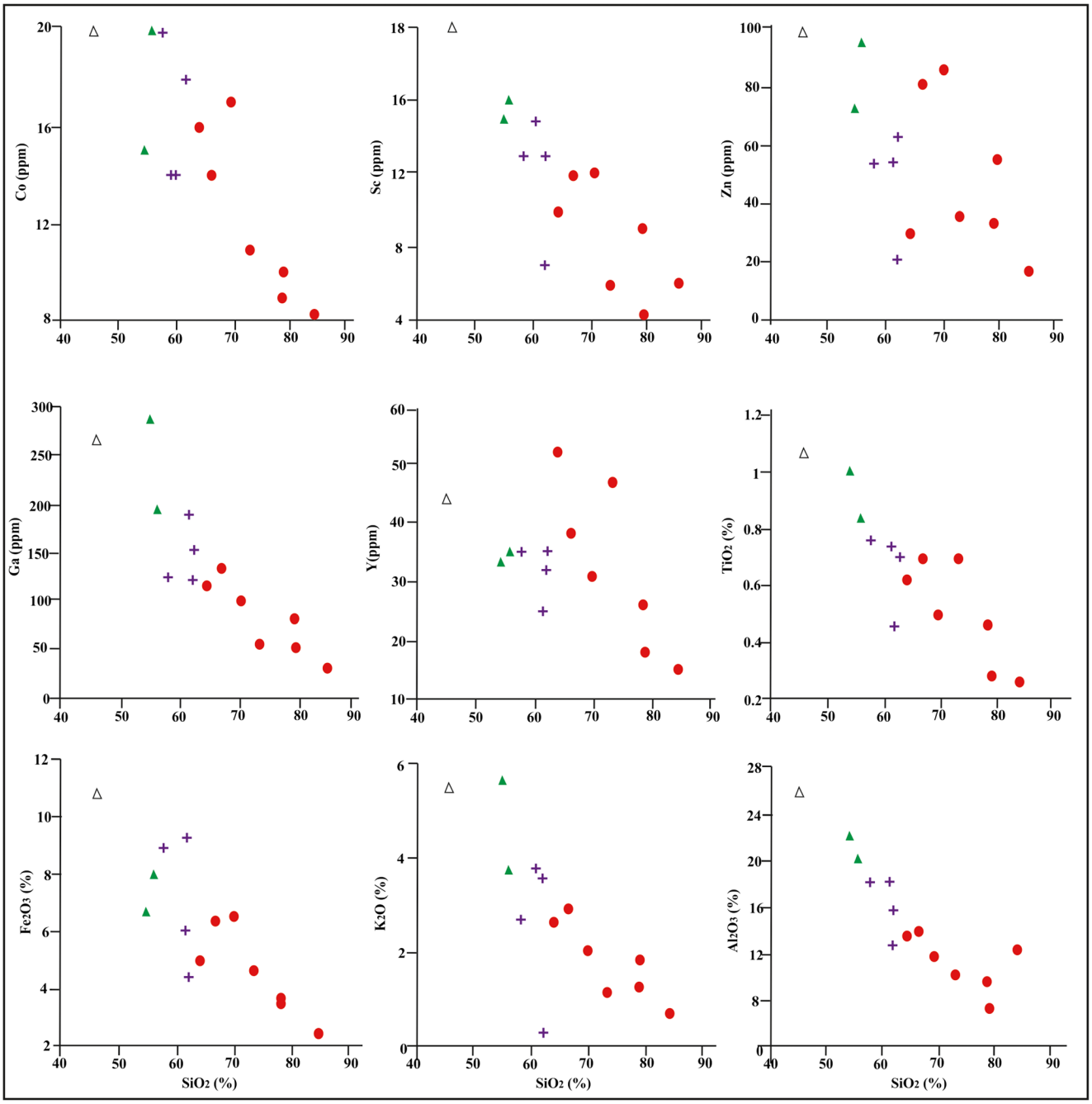

Fig. 3 Major and trace element vs. Si_2O graph showing the distribution of samples from the Neoproterozoic succession of Batal Formation in the Spiti Basin. Sandstone (circles); siltstone (plus signs); shale (filled triangles); phyllite (empty triangles)

igneous source. According to Armstrong-Altrin et al. (2017), the REE pattern and the range of Eu anomalies are highly useful to discriminate mafic and felsic rocks and to interpret the provenance of sediments. In the present study, it was observed that the REE pattern and negative Eu anomaly suggests felsic-type rock as the source rock for Batal Formation. Whereas, LREE enrichment and low HREE pattern reflects that the studied sediments were derived from the silica-recycled sediments or felsic igneous source and deposited on active continental margin.

Based on the molecular composition (Na_2O, CaO, K_2O, and Al_2O_3), few indices of weathering have been proposed

Fig. 4 Major and trace elements vs. Al2O3 graph showing the distribution of samples from the Neoproterozoic succession of Batal Formation. Symbols are as in Fig. 3 ▶

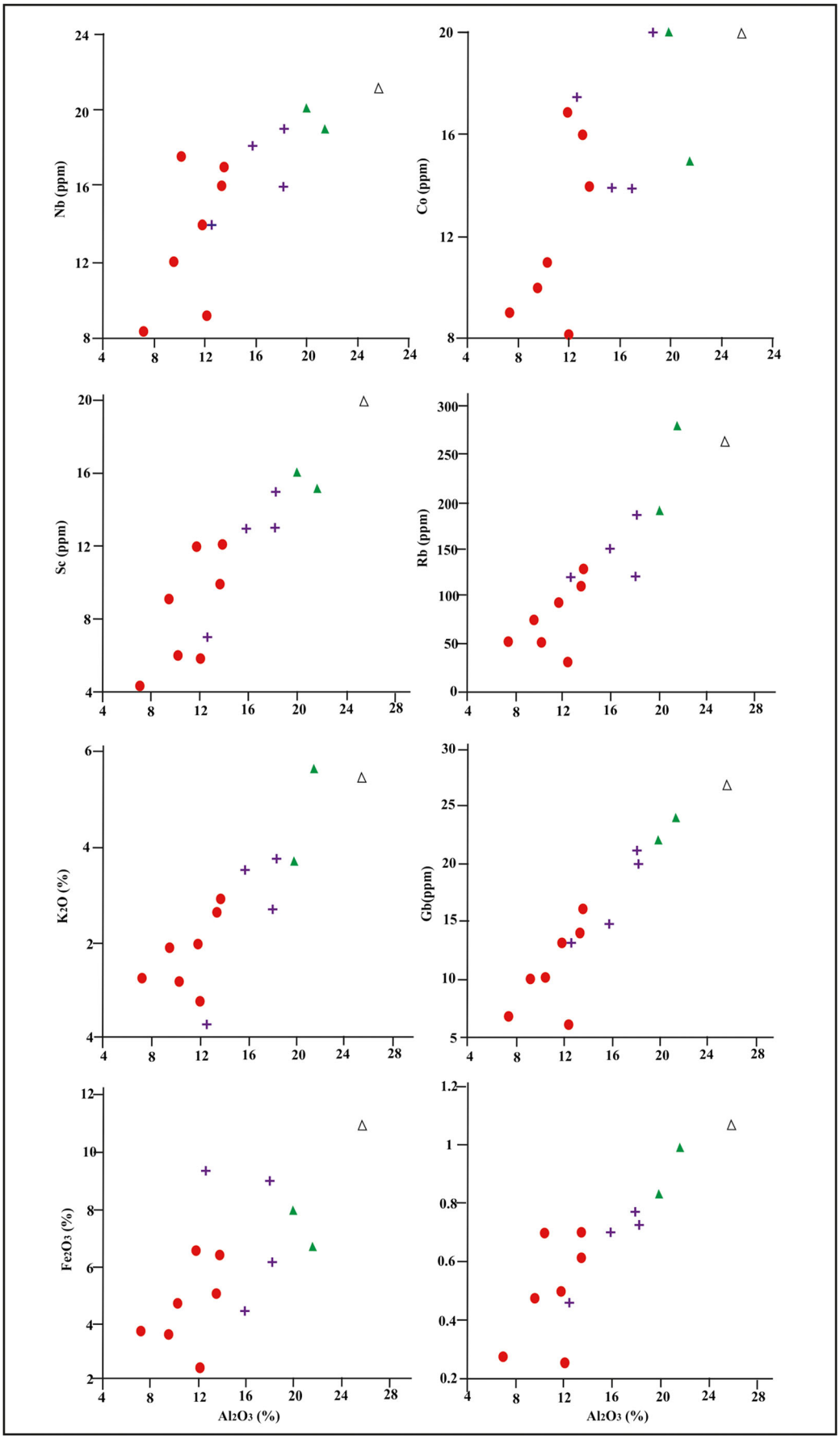
Nb (ppm)
Co (ppm)
Sc (ppm)
Rb (ppm)
K2O (%)
Gb(ppm)
Fe2O3 (%)
Al2O3 (%)
Al2O3 (%)

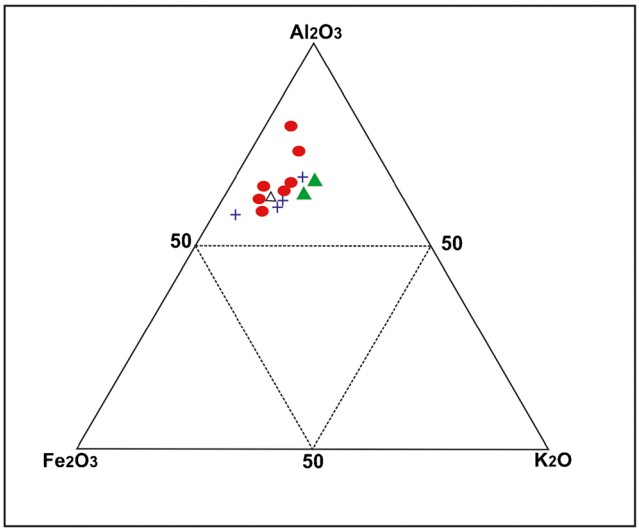

Fig. 5 Major element distribution of Batal Formation in Fe2O3-Al2O3-K2O compositional space by Wronkiewicz and Condie (1987). Symbols as per Fig. 3

to quantify the weathering effects. The most widely used chemical index to quantitatively measure the intensity of source area weathering is the chemical index of alteration (CIA) proposed by Nesbitt and Young (1982). The intensity of weathering in the source area of sediments can be estimated by using CIA (chemical index of alteration). Nesbitt and Young (1982) established the CIA, as $CIA = 100 \times Al_2O_3 / (Al_2O_3 + CaO^* + Na_2O + K_2O)$. In the present study, the analyzed CIA values after Nesbitt and Young (1982) range between 63 and 93 with an average of ~ 72 (Table 1). This suggests that the source area suffered moderate to intensive weathering.

In the A-CN-K ternary plot (Fig. 10), molar proportion of Al_2O_3, Na_2O, and CaO* (CaO in silicate fraction) is plotted to evaluate the mobility of elements during the process of chemical weathering. In the A-CN-K diagram, all the rocks exhibit a definite trend. In the present ternary plot, the rock sample of Batal Formation shows parallel trend to A-CN axis (CIA = 63–93, Fig. 10). The A-CN-K plot shows that the sample falls towards illite composition, which suggests moderate weathering (Fig. 10). The ternary plot source rock composition can be determined by backward projection and parallel to the A-CN line of the weathered samples to a point on the feldspar join (Fedo et al. 1997; Tang et al. 2012). This trend indicates that the sediments were emerging from granite as a potential ultimate source and reaching to the illite stability zone. This suggests that the effects of weathering had not proceeded to the stage of removal of alkali and alkaline earth elements from the clay minerals (Taylor and McLennan 1985). The plot further indicates that the samples were affected by moderate intensity of chemical weathering. In the bivariant plot (Fig. 11) of CIA % against Al_2O_3, 10 samples fall in the region of moderate weathering and four samples fall in the area which indicates the intensive weathering, which further support moderate to intense weathering in the source rock.

Apart from this, some elemental ratio such as K_2O/Al_2O_3, Ni/Co, and Cu/Zn has also been used to define the weathering and provenance. In the present study, the K_2O/Al_2O_3 ratio ranges from 0.02 to 0.26 (Table 1), which shows distribution of samples close to illite line (Cox et al. 1995). This suggests decomposition of K-feldspar and muscovite during weathering under humid climate, and K remains fix in clay (Cox et al. 1995). Redox condition of sediments is indicated by Ni/Co ratio in sedimentary terrain (Dypvik 1984; Dill 1986). The Ni/Co

Table 2 Trace element concentration data of the Neoproterozoic metasedimentary rocks of Batal Formation, Spiti Basin, Tethys Himalaya

Lithology	Sample	Sc	Co	Ni	Cu	Zn	Ga	Pb	Th	Rb	U	Sr	Y	Zr	Nb	Ni/Co	Cu/Zn
Sandstone	B1	12	14	29	51	82	16	12	20	130	3	74	38	274	17	2.07	0.62
Sandstone	B2	9	10	16	54	33	10	8	22	78	3	83	26	226	12	1.60	1.64
Sandstone	B3	4	9	24	40	55	7	22	9	51	1	116	18	130	8	2.67	0.73
Phyllite	B4	20	20	38	66	99	27	5	20	261	5	55	44	245	21	1.90	0.67
Shale	B5	16	20	51	62	95	22	35	18	188	4	86	35	139	20	2.55	0.65
Siltstone	B6	15	14	17	50	54	21	13	20	187	5	81	25	135	16	1.21	0.93
Shale	B7	15	15	23	38	72	24	21	24	279	5	50	33	115	19	1.53	0.53
Sandstone	B8	12	17	31	63	86	13	15	15	94	2	64	31	194	14	1.82	0.73
Siltstone	B9	13	14	35	36	21	15	4	21	150	2	20	32	185	18	2.50	1.71
Sandstone	B10	6	8	22	39	17	6	4	12	30	1	2	15	132	9	2.75	2.29
Sandstone	B11	10	16	55	85	29	14	3	24	113	2	17	52	239	16	3.44	2.93
Siltstone	B12	7	18	28	38	63	13	4	14	120	2	57	35	186	14	1.56	0.60
Siltstone	B13	13	20	36	54	54	20	3	15	122	3	72	35	142	19	1.80	1.00
Sandstone	B14	6	11	16	27	36	10	2	29	52	2	68	47	522	17.6	1.45	0.75

Table 3 Rare earth element concentration data of the Neoproterozoic metasedimentary rocks of Batal Formation, Spiti Basin, Tethys Himalaya

Lithology	Sample	La	Ce	Pr	Nd	Sm	Eu	Gd	Tb	Dy	Ho	Er	Tm	Yb	Lu	Eu*	LREE/HREE
Sandstone	B1	63.81	45.18	30.73	27.02	17.84	9.08	8.27	5.52	7.59	5.53	5.06	7.78	4.84	6.58	0.12	3.06
Sandstone	B2	119.99	92.22	62.60	46.90	27.88	12.80	17.26	14.05	11.40	9.85	9.98	9.53	8.02	7.74	0.05	3.47
Sandstone	B3	75.10	55.82	39.12	29.67	18.16	10.46	11.36	9.86	8.40	7.64	7.77	7.53	6.46	6.45	0.10	2.87
Phyllite	B4	226.16	171.37	121.90	95.64	49.97	25.49	28.54	20.84	14.30	11.15	10.67	9.11	7.40	6.82	0.04	4.95
Shale	B5	124.99	96.92	68.09	53.18	33.77	18.20	21.45	19.74	17.13	15.54	15.43	14.94	12.66	11.58	0.05	2.57
Siltstone	B6	125.98	94.18	67.04	52.46	31.59	16.37	18.48	15.66	11.60	9.01	8.29	7.25	6.11	5.97	0.06	3.76
Shale	B7	146.50	112.47	79.25	58.84	36.19	20.31	22.44	20.36	17.87	16.46	16.67	16.94	14.52	12.95	0.05	2.73
Sandstone	B8	123.91	94.40	68.67	52.77	31.94	15.93	19.33	17.31	14.89	13.41	13.55	13.11	11.51	10.58	0.05	2.87
Siltstone	B9	135.80	102.80	73.34	58.08	34.80	12.17	18.15	12.78	7.74	5.32	5.14	4.22	3.70	3.53	0.04	5.56
Sandstone	B10	64.36	49.93	34.45	26.18	16.00	6.22	9.63	7.91	6.17	5.15	5.16	4.78	4.23	3.87	0.08	3.59
Sandstone	B11	166.40	123.30	90.62	70.60	42.79	13.10	23.50	17.50	11.93	9.11	8.94	7.92	6.67	6.05	0.03	4.72
Siltstone	B12	37.57	30.77	22.18	17.31	11.36	4.75	7.56	6.98	6.26	5.79	5.68	5.56	4.49	4.26	0.11	2.32
Siltstone	B13	128.35	93.56	68.07	52.23	31.52	15.95	17.56	13.38	9.45	7.60	7.56	6.92	6.05	5.79	0.06	4.14
Sandstone	B14	261.58	204.81	140.88	104.08	62.34	22.99	33.01	26.67	21.54	18.91	18.35	17.64	14.62	13.37	0.02	4.14

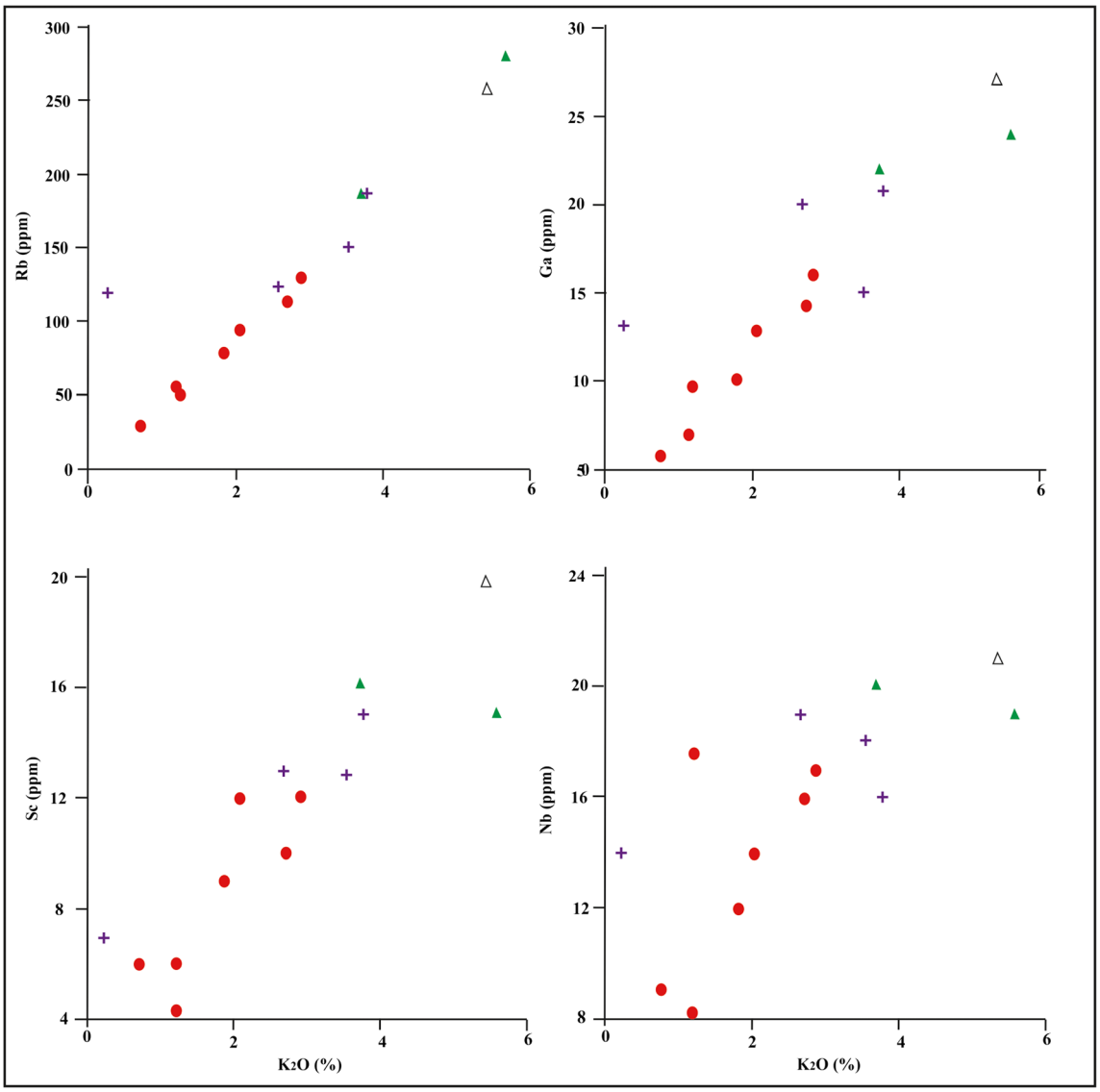

Fig. 6 Trace elements vs. K2O graph showing the distribution of samples from the Neoproterozoic succession of Batal Formation. Symbols are as in Fig. 3

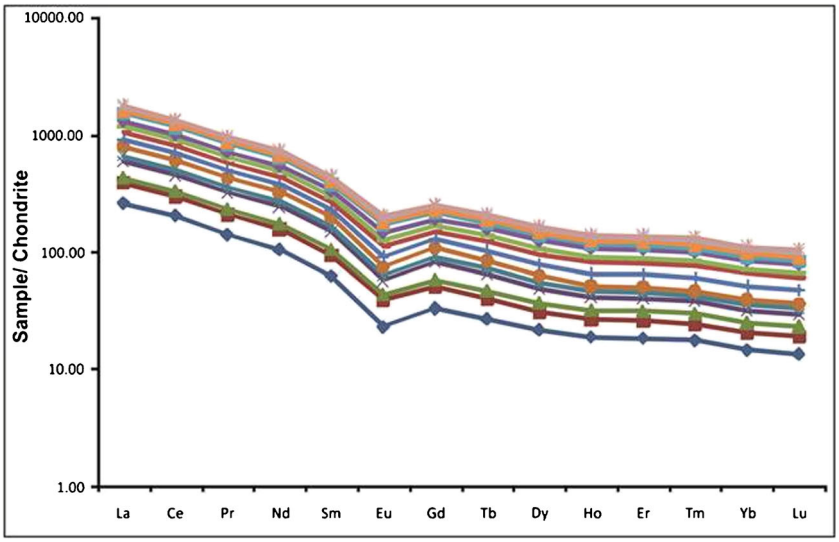

Fig. 7 Chondrite-normalized REE distribution spectra of Neoproterozoic succession of Batal Formation in Spiti Basin

below 5 reflects an aerobic environment, whereas above reflects an anaerobic environment (Jones and Manning 1994). The studied shale and siltstone sample shows Ni/Co ratio (1.2–2.55) which suggests that the sediments were deposited under low to moderate oxygenated environment (Table 2). This is further supported by Cu/Zn ratio as suggested by Hallberg (1976). According to Hallberg (1976), low ratio of Cu/Zn indicates well oxidizing and the high values suggest reducing depositional environment. The low to moderate values of Cu/Zn ratio (0.5–2.9) in the studied samples indicate that the sedimen-

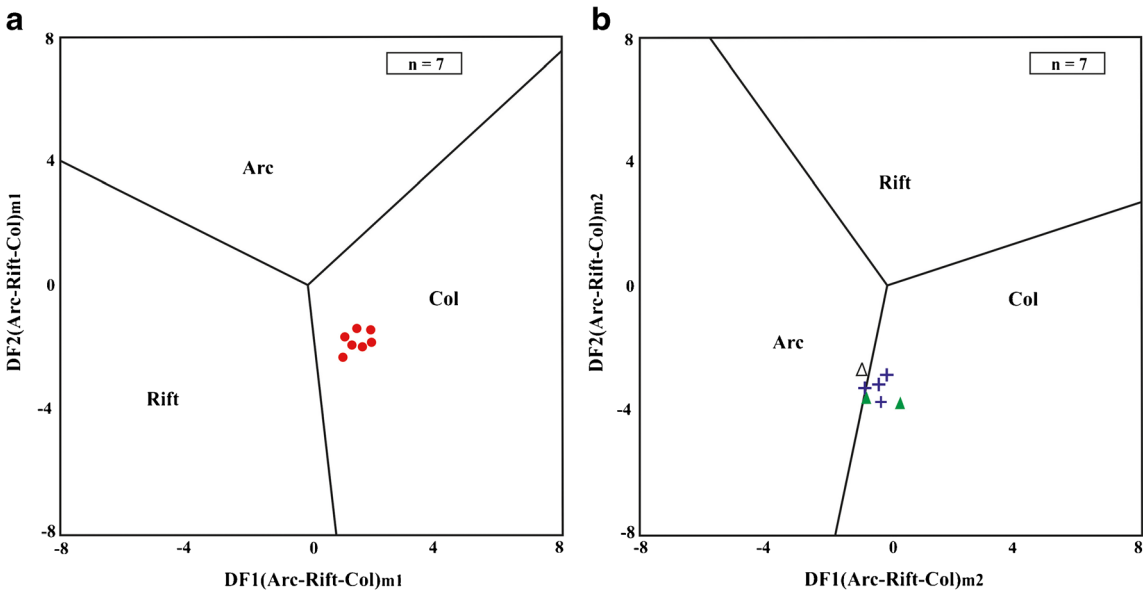

Fig. 8 **a** Discriminant function multidimensional diagram for high-silica clastic sediments (Verma and Armstrong-Altrin 2013). The subscript m1 in DF1 and DF2 represents the high-silica diagram based on log ratios of major elements. The discriminant function equations are DF1(Arc-Rift-Col)m1 = (− 0.263 × In(TiO_2/SiO_2)adj) + (0.604 × In (Al_2O_3/SiO_2)adj) + (− 1.725 × In(Fe_2O_3t/SiO2)adj) + (0.660 × In(MnO/SiO_2)adj) + (2.191 × In(MgO/SiO_2)adj) + (0.144 × In(CaO/SiO_2)adj) + (− 1.304 × In(Na_2O/SiO_2)adj) + (0.054 × In(K_2O/SiO_2)adj) + (− 0.330 × In(P_2O_5/SiO_2)adj) + 1.588; DF2(Arc-Rift-Col)m1 = (− 1.196 × In(TiO_2/SiO_2)adj) + (1.604 × In(Al_2O_3/SiO_2)adj) + (0.303 × In(Fe_2O_3t/SiO_2)adj) + (0.436 × In(MnO/SiO_2)adj) + (0.838 × In(MgO/SiO_2)adj) + (− 0.407 × In(CaO/SiO_2)adj) + (1.021 × In(Na_2O/SiO_2)adj) + (− 1.706 × In(K_2O/SiO_2)adj) + (− 0.126 × In(P_2O_5/SiO_2)adj) − 1.068. **b** Discriminant function multidimensional diagram for low-silica clastic sediments (Verma and Armstrong-Altrin 2013). The subscript m2 in DF1 and DF2 represents the low-silica diagram based on log ratio of major elements. Discriminant function equations are DF1(Arc-Rift-Col)m2 = (0.608 × In(TiO_2/SiO_2)adj) + (− 1.854 × In(Al_2O_3/SiO_2)adj) + (0.299 × In(Fe_2O_3t/SiO_2)adj) + (− 0.550 × In(MnO/SiO_2)adj) + (0.120 × In(MgO/SiO_2)adj) + (0.194 × In(CaO/SiO_2)adj) + (− 1.510 × In(Na_2O/SiO_2)adj) + (1.941 × In(K_2O/SiO_2)adj) + (0.003 × In(P_2O_5/SiO_2)adj) − 0.294; DF2(Arc-Rift-Col)m2 = (− 0.554 × In(TiO_2/SiO_2)adj) + (− 0.995 × In (Al_2O_3/SiO_2)adj) + (1.765 × In(Fe_2O_3t/SiO_2)adj) + (− 1.391 × In(MnO/SiO_2)adj) + (− 1.034 × In(MgO/SiO_2)adj) + (0.225 × In(CaO/SiO_2)adj) + (0.713 × In(Na_2O/SiO_2)adj) + (0.330 × In(K_2O/SiO_2)adj) + (0.637 × In(P_2O_5/SiO_2)adj) − 3.631

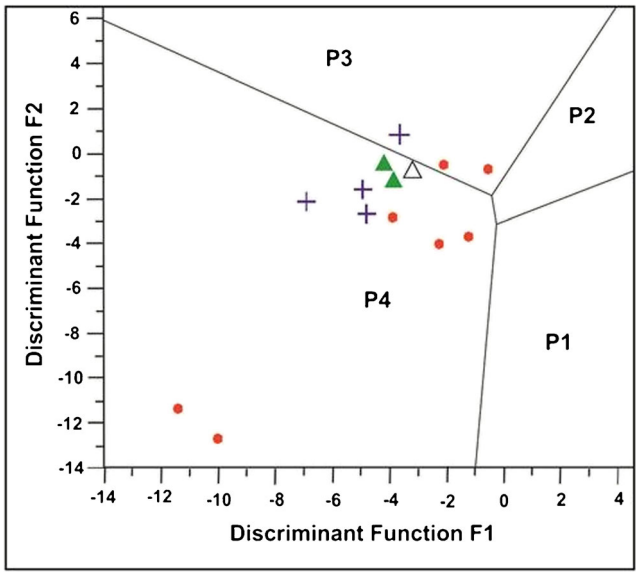

Fig. 9 Discriminant function 1 against discriminant function 2 variation diagram. Fields after Roser and Korsch (1988), wherein Fl = − 1.733TiO2 + 0.607Al2O3 + 0.76Fe2O3 − 1.5MgO + 0.616CaO + 0.509Na2O − 1.224K2O − 9.09 and F2 = 0.445TiO2 + 0.07Al2O3 − 0.25Fe2O3 − 1.142MgO + 0.438CaO + 1.475Na2O + 1.426K2O − 6.86. Provenance fields (P1) mafic igneous provenance, (P2) intermediate igneous provenance, (P3) felsic igneous provenance, and (P4) quartzose sedimentary provenance. Symbols as per Fig. 3

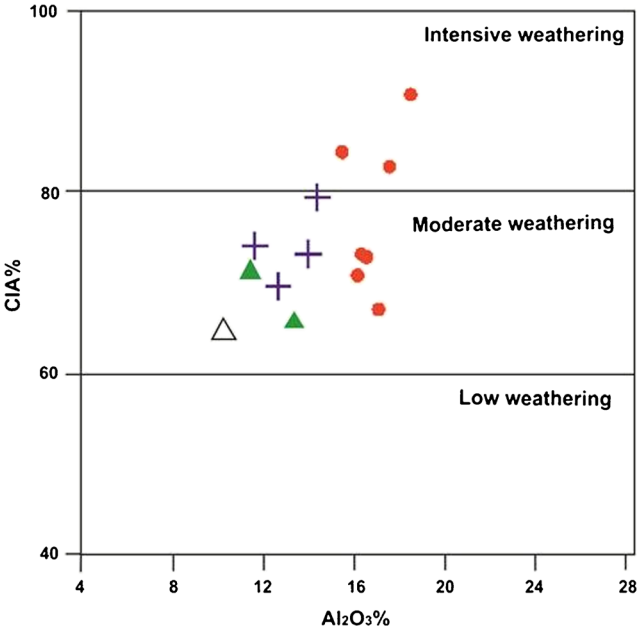

Fig. 11 Bivariant plot of CIA % against Al_2O_3 showing weathering conditions of source rock of the Batal Formation (after Nesbitt and Young 1982)

tary rocks of the Batal Formation were deposited under low to moderate oxidizing condition (Hallberg 1976; Ramos-Vázquez et al. 2017, 2018).

Conclusion

Based on the petrographical and geochemical data of Batal Formation, the following conclusions were derived:

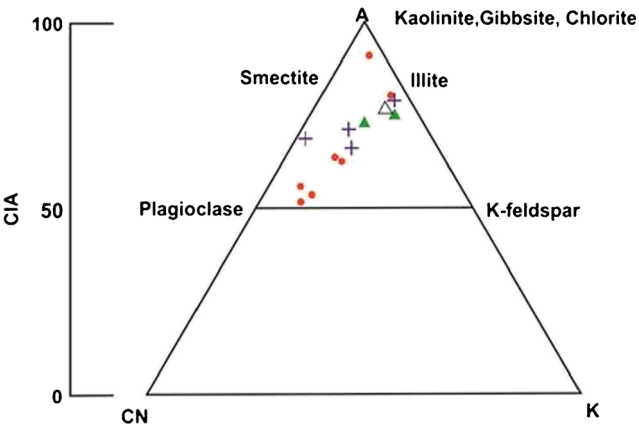

Fig. 10 A-CN-K diagram showing the weathering trend of the siliciclastic rocks (after Nesbitt and Young 1982). **a** Al2O3; CN: CaO∗ + Na2O; K: K2O (molecular composition)

1. The percentage of quartz in sandstone varies from 70 to 80% in siltstone, and in shale, it varies from 50 to 60%; at places, preferred orientation of micaceous minerals was observed.
2. The different major and trace elemental correlation suggests that these elements are primarily controlled by clay minerals.
3. The depletion of HREE, relative with LREE, was due to the lower concentration of heavy minerals, and the REE with negative Eu anomaly indicates felsic source. The significant statistical correlation between Zr versus Yb and ΣHREE represents that these sediments are influenced by sediment recycling.
4. The multidimensional discriminant function diagram indicates that the deposition of sediments took place in active continental marginal environment.
5. The CIA values suggest that the source area suffered moderate to intensive weathering with the presence of clay minerals derived during the cold and dry period.
6. The Ni/Co and Cu/Zn ratio indicates that the rocks of Batal Formation were deposited under low to moderate oxidizing condition.

Acknowledgments We are thankful to the Director, Wadia Institute of Himalayan Geology, Dehradun, for providing facilities and giving permission to publish this work. We are highly thankful to Dr. Hakim Rai for providing his valuable suggestions and scientific inputs to shape the manuscript in the present form. The authors are thankful to the anonymous reviewers for their insightful reviews.

Funding information This work was carried out under the Project SR/FTP/ES-111/20014 funded by the Science and Engineering Board, Department of Science and Technology, Government of India.

References

Ahmad AHM, Noufal KN, Masroor AM, Khan T (2014) Petrography and geochemistry of Jumara dome sediments, Kachchh Basin: implications for provenance, tectonic setting and weathering intensity. Chin J Geochem 33:9–23

Anaya-Gregorio A, Armstrong-Altrin JS, Machain-Castillo ML, Montiel-García PC, Ramos-Vázquez MA (2018) Textural and geochemical characteristics of late Pleistocene to Holocene fine-grained deep-sea sediment cores (GM6 and GM7), recovered from southwestern Gulf of Mexico. J Palaeogeogr 187:3

Armstrong-Altrin JS (2009) Provenance of sands from Cazones Acapulco and Bahia Kino beaches, Mexico. Rev Mex Cienc Geol 26(3):764–782

Armstrong-Altrin JS (2015) Evaluation of two multi-dimensional discrimination diagrams from beach and deep sea sediments from the Gulf of Mexico and their application to Precambrian clastic sedimentary rocks. Int Geol Rev 57(11–12):1446–1461

Armstrong-Altrin JS, Verma SP (2005) Critical evaluation of six tectonic setting discrimination diagrams using geochemical data of Neogene sediment from known tectonic settings. Sediment Geol 177:115–129

Armstrong-Altrin JS, Lee YI, Kasper-Zubillaga JJ, Carranza-Edwards A, Garcia D, Eby N, Balaram V, Cruz-Ortiz NL (2012) Geochemistry of beach sands along the Western Gulf of Mexico: implication for provenance. Chem Erde - Geochem 72:345–362

Armstrong-Altrin JS, Nagarajan R, Madhavaraju J, Rosalez-Hoz L, Lee YI, Balaram V, Cruz-Martínez A, Avila-Ramírez G (2013) Geochemistry of the Jurassic and UpperCretaceous shales from the Molango Region, Hidalgo, eastern Mexico: implications for source-area weathering, provenance, and tectonic setting. Comptes Rendus Geosci 345:185–202

Armstrong-Altrin JS, Machain-Castillo ML, Rosales-Hoz L, Carranza-Edwards A, Sanchez-Cabeza JA, Ruíz-Fernández AC (2015a) Provenance and depositional history of continental slope sediments in the Southwestern Gulf of Mexico unraveled by geochemical analysis. Cont Shelf Res 95:15–26

Armstrong-Altrin JS, Nagarajan R, Balaram V, Natalhy-Pineda O (2015b) Petrography and geochemistry of sands from the Chachalacas and Veracruz beach areas, western Gulf of Mexico, Mexico: constraints on provenance and tectonic setting. J S Am Earth Sci 64:199–216

Armstrong-Altrin JS, Lee YI, Juan J, Kasper-Zubillaga J, Trejo-Ramírez E (2017) Mineralogy and geochemistry of sands along the Manzanillo and El Carrizal beach areas, southern Mexico: implications for palaeoweathering, provenance and tectonic setting. Geol J 52:559–582

Armstrong-Altrin JS, Ramos Vázquez MA, Zavala-León AC, Montiel-García PC (2018) Provenance discrimination between Atasta and Alvarado beach sands, western Gulf of Mexico, Mexico: constraints from detrital zircon chemistry and U–Pb geochronology. Geol J. https://doi.org/10.1002/gj.3122

Bau M, Dulski P (1996) Distribution of yttrium and rare-earth elements in the Penge and Kuruman iron-formations, Transvaal Supergroup, South Africa. Precambrian Res 79:37–55

Bhargava ON (2008a) Paleozoic successions of Indian plate; Geol. Soc India Memoir 74:209–244

Bhargava ON (2008b) An update of introduction to the Spiti geology. J Palaeontol Soc India 53(2):113–128

Bhatia MR (1983) Plate tectonics and geochemical composition of sandstones. J Geol 91:611–627

Bhatia MR, Cook KAW (1986) Trace element characteristics of graywackes and tectonic setting discrimination of sedimentary basins. Contrib Mineral Petrol 92:181–193

Cox R, Low DR, Cullers RL (1995) The influence of sediment recycling and basement composition on evolution of mudrock chemistry in the southwestern United States. Geochim Cosmochim Acta 59: 2919–2940

Cullers R L (1994) The controls on the major and trace element variation of shale, siltstone and sandstone of Pennsylvanian- Permian age from uplifted continental blocks in Colorado to platform sediment in Kansas, USA. Geochimica et Cosmochica Acta. 58:4955–4972

Cullers RL, Graf J (1983) Rare earth elements in igneous rocks of the continental crust: intermediate and silicic rocks, ore petrogenesis. In: Henderson P (ed) Rare-Earth Geochemistry. Elsevier, Amsterdam, pp 275–312

Cullers RL, Bock B, Guidotti C (1997) Elemental distributions and neodymium isotopic compositions of Silurian metasediments, western Maine, USA: redistribution of the rare earth elements. Geochim Cosmochim Acta 61:1847–1861

Dabard MP (1990) Lower Brioverian formations (Upper Proterozoic) of the Armorican Massif (France): geodynamic evolution of source areas revealed by sandstone petrography and geochemistry. Sediment Geol 69:45–58

Dill H (1986) Metallogenesis of early Paleozoic graptolite shales from the Graefenthal Horst (northern Bavaria-Federal Republic of Germany). Econ Geol 81:889–903

DiPietro JA, Pogue KR (2004) Tectonostratigraphic subdivisions of the Himalaya: a view from the west. Tectonics 23:1–20

Dragnits E (2000) The Muth Formation in the Pin Valley (Spiti, N-India): depositional environment and ichnofauna of a Lower Devonian barrier island system. Ph D Thesis, University of Vienna. 144 pp

Dypvik H (1984) Geochemical compositions and depositional conditions of Upper Jurassic and Lower Cretaceous Yorkshire clays, England. Geol Mag 121(5):489–504

Fedo CM, Young GM, Nesbitt GM (1997) Paleoclimatic control on the composition of the Paleoproterozoic Serpent Formation, Huronian Supergroup, Canada: a greenhouse to icehouse transition. Precambrian Res 86:201–223

Frank W, Grasemann B, Guntili P, Miller C (1995) Geological map of the Kishtwar, Chamba anf Kulu region, NW Himalaya, India. Jahrb Geol Bundesanst 138:299–308

Fu X, Wang J, Zeng Y, Tan F, Feng X (2010) REE geochemistry of marine oil shale from the Changshe Mountain area, northern Tibet, China. Int J Coal Geol 81:191–199

Govindaraju K (1994) Compilation of working values and sample description for 383 geostandards. Geostand Newslett 18:158

Griesbach CL (1891) Geology of the Central Himalayas. Mem Geol Surv India 23:1–232

Hallberg RO (1976) A geochemical method for investigation of palaeoredox conditions in sediments: Ambio. Spec Rep 4:139–147

Hayden HH (1904) The geology of the Spiti with parts of Bashahr and Rupshu. Mem Geol Surv India Mem 36(1):1–129

Hernández-Hinojosa V, Montiel-García PC, Armstrong-Altrin JS, Nagarajan R, Kasper-Zubillaga JJ (2018) Textural and geochemical characteristics of beach sands along the Western Gulf of Mexico, Mexico. Carpathian J Earth Environ Sciences 13(1):161–174

Jones B, Manning DAC (1994) Comparison of geochemical indices used for the interpretation of paleoredox conditions in ancient mudstones. Chem Geol 111:111–129

Kumar G, Raina BK, Bhargava ON, Maithy PK, Babu R (1984) The Precambrian-Cambrian boundary problem and its prospects, northwest Himalaya, India. Geol Mag 121(3):211–219

Madhavaraju J (2015) Geochemistry of Campanian–Maastrichtian sedimentary rocks in the Cauvery basin, south India; In: Ramkumar M

(ed) Constraints on paleoweathering, provenance and Cretaceous environments. Chemostratigraphy: Concepts, Techniques and Applications, Elsevier Spec. pp 185–214

Madhavaraju J, Lee YI (2010) Influence of Deccan volcanism in the sedimentary rocks of late Maastrichtian–Danian age of Cauvery basin, southeastern India: constraints from Geochemistry. Curr Sci 98:528–537

Madhavaraju J, González-León C M, Yong Il Lee, Armstrong-Altrin J S, Reyes-Campero L M, (2010) Geochemistry of the Mural Formation (Aptian-Albian) of the Bisbee Group, Northern Sonora, Mexico: Cretaceous Research 31:400–414

Madhavaraju J, Erik Ramirez-Montoya E, Monreal R, González-Leon CM, Pi-Puig T, Espinoza-Maldonado IG, Grijalva-Noriega FJ (2016) Paleoclimate, paleoweathering and paleoredox conditions of Lower Cretaceous shales from the Mural Limestone, Tuape section, northern Sonora, Mexico: Constraints from clay mineralogy and geochemistry. Rev Mex Cienc Geol 33(1):34–48

McLennan SM, Taylor SR (1991) Sedimentary rocks and crustal evolution: tectonic setting and secular trends. J Geol 99:1–21

McLennan SM, Hemming S, McDaniel DK, Hanson GN (1993) Geochemical approaches to sedimentation, provenamce and tectonics. In: Johnson MJ, Basu A (eds) Processes controlling the composition of clastic sediments. Geological Society of America Special Paper, USA, pp 21–40

Myrow PM, Thompson KR, Hughes NC, Paulsen TS, Sell BK, Parcha SK (2006) Cambrian stratigraphy and depositional history of the northern Indian Himalaya, Spiti Valley, north-Central India. Geol Soc Am 18(3–4):491–510

Myrow PM, Hughes NC, Goodge JW, Fanning CM, Williams IS, Peng S, Bhargava ON, Parcha SK, Pogue KR (2010) Extraordinary transport and mixing of sediment across Himalayan Central Gondwana during the Cambrian–Ordovician. Geol Soc Am Bull 122(9–10):1660–1670

Nagarajan R, Madhavaraju J, Nagendra R, Armstrong-Altrin JS, Moutte J (2007a) Geochemistry of Neoproterozoic shales of the Rabanpalli formation, Bhima basin, northern Karnataka, southern India: implications for provenance and paleoredox conditions; rev. Mex Cienc Geol 24:150–160

Nagarajan R, Armstrong-Altrin JS, Nagendra R, Madhavaraju J, Moutte J (2007b) Petrography and geochemistry of terrigenous sedimentary rocks in the Neoproterozoic Rabanpalli formation, Bhima basin, southern India: implications for paleoweathering condition, provenance, and source rock composition. J Geol Soc India 70:297–312

Nagarajan R, Armstrong-Altrin JS, Kessler FL, Jong J (2017) Petrological and geochemical constraints on provenance, paleoweathering and tectonic setting of clastic sediments from the Neogene Lambir and Sibuti formations, northwestern Borneo. In: Mazumder R (ed) Sediment provenance. Elsevier, Amsterdam, pp 123–153

Nesbitt HW, Young GM (1982) Early Proterozoic climates and plate motions inferred from major element chemistry of lutites. Nature 299:715–717

Nyakairu GWA, Koeerl C (2001) Mineralogical and chemical composition and distribution of rare earth elements in clay-rich sediments from Central Uganda; Geochem. J 35:13–28

Pandey S, Parcha SK (2017) Provenance, tectonic setting and source-area weathering of the lower Cambrian sediments of the Parahio valley in the Spiti basin. India J Earth Syst Sci 126(27)

Ramos-Vázquez M, Armstrong-Altrin JS, Rosales-Hoz L, Machain-Castillo ML, Carranza-Edwards A (2017) Geochemistry of deep-sea sediments in two cores retrieved at the mouth of the Coatzacoalcos river delta, Western Gulf of Mexico. Mex Arab J Geosci 10(6):148

Ramos-Vázquez M, Armstrong-Altrin JS, Machain-Castillo ML, Gío-Argáez FR (2018) Foraminiferal assemblages, 14C ages, and compositional variations in two sediments cores in the western Gulf of Mexico. J S Am Earth 88:480–496

Roser BP, Korsch RJ (1986) Determination of tectonic setting of sandstone-mudstone suites using SiO_2 content and K_2O/Na_2O ratio. J Geol 94:635–650

Roser B P, Korsch R J (1988) Provenance signatures of sandstone-mudstone suites determined using discrimination function analysis of major-element data. Chemical Geology 67:119–39

Sari A, Koca D (2012) An approach to provenance, tectonic and redox conditions of Jurassic– cretaceous Akkuyu formation, central Taurids, Turkey. Min Res Explor Bull 144:51–74

Srikantia SV (1981) The Lithostratigraphy, sedimentation and structure of the Proterozoic-Phanerozoic formations of Spiti basin in the higher Himalayas of Himachal Pradesh India. In: Sinha AK (ed) Contemporary geoscientific research in Himalaya, vol 1. Bishen Singh Mahendra Pal Publisher, Dehradun, pp 31–38

Srikantia SV, Bhargava ON (1998) Geology of Himachal Pradesh. Geological Society of India. 406 pp

Tang Y, Sang L, Yuan Y, Zhang Y, Yang Y (2012) Geochemistry of late Triassic pelitic rocks in the NE part of Songpan–Ganzi basin, western China: implications for source weathering, provenance and tectonic setting. Geosci Front 3(5):647–660

Taylor SR, McLennan SM (1985) The continental crust: its composition and evolution. Blackwell Scientific, Oxford 312 p

Thakur VC (1980) Tectonics of the central crystallines of western Himalaya. Tectonophysics 62(1–2):141–154

Tobia FH, Aswad KJ (2015) Petrography and geochemistry of Jurassic sandstones, western desert, Iraq: implications on provenance and tectonic setting. Arab J Geosci 8:2771–2784

Verma SP, Armstrong-Altrin JS (2013) New multi-dimensional diagrams for tectonic discrimination of siliciclastic sediments and their application to Precambrian basins. Chem Geol 355:117–180

Wronkiewicz DJ, Condie KC (1987) Geochemistry of Archean shales from the Witwatersrand Supergroup, South Africa: source-area weathering and provenance. Geochim Cosmochim Acta 51:2401–2416

Zaid SM (2015b) Integrated petrographic, mineralogical, and geochemical study of the late cretaceous-early tertiary Dakhla shales, Qusier-Nile valley province, Central Egypt: implications for source area weathering, provenance, and tectonic setting. Arab J Geosci 8: 9237–9259

Zaid SM (2015c) Geochemistry of sandstone from the Pliocene Gabir formation, north Marsa Alam, Red Sea, Egypt: implication for provenance, weathering and tectonic setting. J Afr Earth Sci 102:1–17